

# Bars in low-density environments rotate faster than bars in dense regions

Natalia Puczek,<sup>1</sup> Tobias Géron,<sup>1,2</sup> Rebecca J. Smethurst<sup>1</sup> and Chris J. Lintott<sup>1\*</sup>

<sup>1</sup>*Oxford Astrophysics, Department of Physics, University of Oxford, Denys Wilkinson Building, Keble Road, Oxford OX1 3RH, UK*

<sup>2</sup>*Dunlap Institute for Astronomy & Astrophysics, University of Toronto, 50 St. George Street, Toronto ON M5S 3H4, Canada*

Accepted XXX. Received YYY; in original form ZZZ

arXiv:2511.02054v1 [astro-ph.GA] 3 Nov 2025

## ABSTRACT

Does the environment of a galaxy directly influence the kinematics of its bar? We present observational evidence that bars in high-density environments exhibit significantly slower rotation rates than bars in low-density environments. Galactic bars are central, extended structures composed of stars, dust and gas, present in approximately 30 to 70 per cent of luminous spiral galaxies in the local Universe. Recent simulation studies have suggested that the environment can influence the bar rotation rate,  $\mathcal{R}$ , which is used to classify bars as either fast ( $1 \leq \mathcal{R} \leq 1.4$ ) or slow ( $\mathcal{R} > 1.4$ ). We use estimates of  $\mathcal{R}$  obtained with the Tremaine–Weinberg method applied to Integral Field Unit spectroscopy from MaNGA and CALIFA. After cross-matching these with the projected neighbour density,  $\log \Sigma$ , we retain 286 galaxies. The analysis reveals that bars in high-density environments are significantly slower (median  $\mathcal{R} = 1.67^{+0.72}_{-0.42}$ ) compared to bars in low-density environments (median  $\mathcal{R} = 1.37^{+0.51}_{-0.34}$ ); Anderson–Darling  $p$ -value of  $p_{AD} = 0.002$  ( $3.1\sigma$ ). This study marks the first empirical test of the hypothesis that fast bars are formed by global instabilities in isolated galaxies, while slow bars are triggered by tidal interactions in dense environments, in agreement with predictions from numerous  $N$ -body simulations. Future studies would benefit from a larger sample of galaxies with reliable Integral Field Unit data, required to measure bar rotation rates. Specifically, more data are necessary to study the environmental influence on bar formation within dense settings (i.e. groups, clusters and filaments).

**Key words:** galaxies: bar – galaxies: kinematics and dynamics – galaxies : evolution – galaxies: structure – galaxies: statistics – galaxies : formation

## 1 INTRODUCTION

A bar in a galaxy is a central, extended, long-lived structure composed of stars, dust and gas, present in approximately 30 to 70 per cent of luminous spiral galaxies in the local Universe, with the bar fraction depending on factors such as bar strength, wave-band in which it is observed, galaxy colour and mass (Eskridge et al. 2000; Sheth et al. 2008; Masters et al. 2011; Erwin 2018; Géron et al. 2021). Although *JWST* has now detected bars beyond  $z \sim 3$  (a look-back time of 11.5 Gyr; Costantin et al. 2023; Smail et al. 2023; Amvrosiadis et al. 2025; Géron et al. 2025), simulations mark the epoch of bar formation to be around  $z \sim 0.7$ –1, coinciding with the galaxies’ transition to being dynamically cool and disc-dominated and a decline in major mergers (Kraljic, Bournaud & Martig 2012; Melvin et al. 2014). In this secular epoch, slow processes become more dominant in galaxy evolution, providing a stable environment for bars to form and persist over long timescales.

Galactic bars are thought to play a critical role in galaxy evolution, funnelling gas to the centre of the galaxy, triggering starbursts and facilitating quenching (Masters et al. 2012; Cheung et al. 2013; Kruk et al. 2018; Géron et al. 2021). Bars allow mass and angular momentum redistribution, stabilizing stellar orbits and influencing subsequent evolution of disc galaxies (Ostriker & Peebles 1973; Combes 2009; Sellwood 2012). Therefore, studying bars is pivotal to building a coherent description of galaxy dynamics.

Both galaxy stellar mass and dark matter halo mass have been suggested as important factors in bar formation and evolution (Fujii et al. 2018; Rosas-Guevara et al. 2020; Kumar, Das & Kataria 2022; Bland-Hawthorn et al. 2023). Although some studies argue that bar formation and evolution are predominantly influenced by the internal processes of the host galaxy (Sarkar, Pandey & Bhattacharjee 2021; Aguerri et al. 2023), the dynamical impact of events such as flybys, minor mergers and satellite interactions on the formation and evolution of barred galaxies has been extensively studied (Kyzliopoulos et al. 2016; Moitazedian et al. 2017; Cavanagh & Bekki 2020; Ghosh et al. 2021). It has long been established that bar formation can be triggered by either tidal interactions (Noguchi 1987; Lang, Holley-Bockelmann & Sinha 2014; Lokas et al. 2016; Gajda, Lokas & Athanassoula 2017; Lokas 2018) or by internal instabilities in cold isolated discs (Hohl 1971; Ostriker & Peebles 1973; Athanassoula, Machado & Rodionov 2013; Sellwood 2014). Simulations further show that tidal interactions can trigger bar formation in galaxies, which would have not otherwise been able to form a bar in isolation (Miwa & Noguchi 1998; Lang et al. 2014; Martinez-Valpuesta et al. 2017). While the internal dynamics and morphologies of hosts are an important factor in the study of bars, bar formation and evolution are also strongly linked to the environment of the galaxy.

However, observational evidence for a relationship between environmental density and bar pattern speed has been lacking. Bar pattern speed,  $\Omega_{\text{bar}}$ , is a fundamental parameter of a bar, as it measures the

\* E-mail: cjl@astro.ox.ac.uk (CJL)

angular frequency of the bar's rotation about the galactic centre. Given the variation in galaxy sizes, bar pattern speed is normally parametrised by the bar rotation rate, defined as the dimensionless ratio of the bar's corotation radius,  $R_{\text{cr}}$ , and its semi-major axis,  $R_{\text{bar}}$  (Cuomo et al. 2019), that is

$$\mathcal{R} = \frac{R_{\text{cr}}}{R_{\text{bar}}}. \quad (1)$$

The corotation radius is the radius at which the bar and the stars in the disc rotate at the same speed. The bar rotation rate parameter is used to classify bars as either slow ( $\mathcal{R} > 1.4$ ) or fast ( $1 \leq \mathcal{R} \leq 1.4$ ), with the median value of  $\mathcal{R}$  being around 1.66 (Géron 2023). Slow bars fall short of  $R_{\text{cr}}$ , while fast bars extend out to the corotation radius and their pattern speeds are close to the maximum rotation speed allowed at a given bar length. Despite ultrafast bars ( $\mathcal{R} < 1$ ) being unphysical (Contopoulos 1980), they are repeatedly measured observationally (Rautiainen, Salo & Laurikainen 2008; Font et al. 2017; Guo et al. 2019). This is likely a measurement artefact, as the ultrafast bar phenomenon essentially disappears when bar radius is measured carefully (Cuomo et al. 2019). In this paper, we refer to all bars with  $\mathcal{R} \leq 1.4$  as fast.

*N*-body simulations indicate that bars triggered by instabilities within the discs of isolated galaxies are typically fast, whereas bars formed due to tidal interactions are slow (Miwa & Noguchi 1998; Berentzen et al. 2004; Lokas et al. 2014, 2016; Martinez-Valpuesta et al. 2017; Gajda et al. 2017; Lokas 2018). Simulations show that bar evolution in isolated galaxies proceeds through three distinct phases. Once the bar emerges, it continues to grow in the vertical direction for the first  $\sim 2$  Gyr, after which it buckles (bends out of the galactic disc forming a boxy/peanut bulge) becoming shorter and weaker for the next  $\sim 1$  Gyr (Combes & Sanders 1981; Raha et al. 1991; Martinez-Valpuesta & Shlosman 2004). Eventually it enters a phase during which it slows down and gradually grows in length and strength over several Gyr (Raha et al. 1991; Martinez-Valpuesta, Shlosman & Heller 2006; Athanassoula 2013; Sellwood 2014).  $\mathcal{R}$  fluctuates across all three stages, but in general,  $\mathcal{R} \lesssim 1.4$  for most of the time (Miwa & Noguchi 1998; Berentzen et al. 2004; Martinez-Valpuesta et al. 2017). Simulations of bars influenced or triggered by tidal interactions (i.e. tidal bars) indicate that tidal bars initially undergo weak buckling, after which their rotation rates,  $\mathcal{R}$ , decrease gradually for  $\sim 4$  Gyr (Miwa & Noguchi 1998; Martinez-Valpuesta et al. 2017; Gajda et al. 2017; Lokas 2018), such that the bars eventually enter the fast regime, with  $\mathcal{R} \sim 1.4$  (Martinez-Valpuesta et al. 2017). Nonetheless, for most of the time, tidal bars are very slow, with  $\mathcal{R} \sim 2 - 3$  (Miwa & Noguchi 1998; Berentzen et al. 2004; Lokas et al. 2014, 2016; Gajda et al. 2017; Lokas 2018). Miwa & Noguchi (1998) suggest angular CA g transfer to the perturber as a possible explanation for this slow rotation.

Therefore,  $\mathcal{R}$  could be an observational parameter which distinguishes between tidal bars and bars triggered by internal instabilities. Lokas et al. (2016) simulated bar formation on different orbits in a cluster, demonstrating that tidal interactions can trigger or influence bar formation in cluster cores but not in cluster outskirts. Similarly, tidal features in galaxies have been shown to be more frequent in groups and clusters compared to isolated galaxies (Fried 1988). Therefore, we expect that a higher environmental density would lead to a higher fraction of tidal bars. We hypothesise that measurements of bar rotation rate and environmental density should reveal a positive correlation between the two variables. This study is the first observational test of this hypothesis.

To determine whether the simulation results are confirmed by observational data, we use estimates of the rotation rate,  $\mathcal{R}$ , obtained for 334 galaxies in the local Universe using the Tremaine–Weinberg method applied to Integral Field Unit (IFU) spectroscopy from Mapping Nearby Galaxies at Apache Point Observatory (MaNGA; Bundy et al. 2015) and Calar Alto Legacy Integral Field Area (CALIFA; Sánchez et al. 2012) surveys, across six studies (Aguerri et al. 2015; Guo et al. 2019; Cuomo et al. 2019; Garma-Oehmichen et al. 2020, 2022; Géron et al. 2023). We cross-match these with projected neighbour densities,  $\log_{10}(\Sigma/\text{Mpc}^{-2})$  (i.e.  $\log \Sigma$ ), from Baldry et al. (2006) using a 10 arcsec search radius, retaining 286 galaxies. To test whether galaxy stellar mass could be responsible for variations in  $\mathcal{R}$ , we additionally cross-match the  $\log \Sigma$  sample with stellar masses,  $\log_{10}(M_{\star}/\text{M}_{\odot})$  (i.e.  $\log M_{\star}$ ), from the MPA-JHU collaboration (Max-Planck Institute for Astrophysics & John Hopkins University; Kauffmann et al. 2003), retaining 275 galaxies. This marks the first empirical test of the assumption that fast bars are formed by global instabilities in the galactic discs of isolated galaxies, while slow bars are triggered by tidal interactions in dense environments.

This paper proceeds as follows: In Section 2 we provide a detailed description of our data sources and galaxy sample. In Section 3 we present the measured relationships between  $\mathcal{R}$ ,  $\log \Sigma$  and  $\log M_{\star}$ . We discuss the results in Section 4. Finally, we summarise our findings in Section 5.

## 2 DATA

We obtain the dimensionless  $\mathcal{R}$  measurements for 210 galaxies from Géron et al. (2023), who applied the model-independent kinematic Tremaine–Weinberg (TW) method based on the work of Tremaine & Weinberg (1984) to line-of-sight stellar velocity and stellar flux measurements. The TW method measures the bar pattern speed,  $\Omega_{\text{bar}}$ , by calculating the velocity component misalignment with the major axis of the galaxy. To determine the corotation radius, Géron et al. (2023) combined their measurements of  $\Omega_{\text{bar}}$  with galaxy rotation curves derived from stellar velocity data. For each galaxy, the authors multiplied  $\Omega_{\text{bar}}$  by a range of radii, obtaining a measure of the bar's speed as a function of radius. The radius at which this curve intersected the galaxy rotation curve was the corotation radius. Géron et al. (2023) subsequently combined their measurements of  $R_{\text{cr}}$  with manual bar length measurements to calculate  $\mathcal{R}$ . The authors obtained stellar velocity and stellar flux data from MaNGA IFU in the seventeenth data release of the Sloan Digital Sky Survey (SDSS; Abdurro'uf et al. 2022). Additionally, they made use of Galaxy Zoo DESI (Walmsley et al. 2023) to identify barred galaxies in the IFU survey.

Géron et al. (2023) provide the largest sample of kinematically classified bars to date. However, given the rigorous constraints on data necessary for the TW method, this is still only a small fraction of bars observed by MaNGA. Specifically, the method can only be applied to galaxies with intermediate inclinations ( $20^\circ < i < 70^\circ$ ), since edge-on galaxies do not have accurate spatial measurements, while face-on galaxies lack accurate stellar velocity measurements. Additionally, the bar may not be aligned with the axes of the galaxy, presenting an additional constraint (Tremaine & Weinberg 1984; Géron et al. 2023). As a result, the authors were able to retain only 2 per cent of MaNGA barred galaxies identified by Galaxy Zoo DESI. Therefore, we supplement the galaxy sample with  $\mathcal{R}$  measurements from five other studies which also applied the TW method, retaining only the most recent  $\mathcal{R}$  estimate in cases of duplicates, in the same order as they appear in Table 1. This results in a sample containing 334

**Table 1.** Summary of the bar rotation studies used in our study. The table outlines the IFU spectroscopy catalogue used in the studies and the number of galaxies added to our bar rotation rate, projected neighbour density and galaxy stellar mass samples.

Study	Catalogue	$\mathcal{R}$	$\log \Sigma$	$\log M_\star$
Géron et al. (2023)	MaNGA	210	190	185
Garma-Oehmichen et al. (2022)	MaNGA	56	51	46
Garma-Oehmichen et al. (2020)	MaNGA & CALIFA	6	3	3
Cuomo et al. (2019)	CALIFA	16	9	9
Guo et al. (2019)	MaNGA	34	28	27
Aguerri et al. (2015)	CALIFA	12	5	5
<b>TOTAL</b>		334	286	275

galaxies with measured  $\mathcal{R}$ . Our sample covers the local Universe, with a redshift range  $0.017 < z < 0.078$ .

We use the dimensionless projected neighbour density,  $\log_{10} (\Sigma/\text{Mpc}^{-2})$ , from Baldry et al. (2006), as a measure of environmental density (measured using spectroscopy from the seventh release of SDSS; Abazajian et al. 2009). The projected neighbour density is available for 286 galaxies from our original sample.  $\log \Sigma$  is derived by averaging  $\log_{10} (\Sigma_N/\text{Mpc}^{-2})$  for  $N = 4$  and 5, where

$$\Sigma_N = \frac{N}{\pi d_N^2}, \quad (2)$$

and  $d_N$  [Mpc] is the distance to the  $N^{\text{th}}$  nearest neighbour. A larger (smaller) value of  $\log \Sigma$  corresponds to a denser (less dense) environment.

Additionally, we use the dimensionless logarithmic median total stellar masses,  $\log_{10} (M_\star/\text{M}_\odot)$ , from the MPA-JHU collaboration (Kauffmann et al. 2003). The authors derived the masses through fits to the seventh release of SDSS photometry (Abazajian et al. 2009). Stellar masses are available for 275 galaxies from the  $\log \Sigma$  sample described in the previous paragraph.

In Section 3, we investigate the dependence of the bar rotation rate on projected neighbour density and galaxy stellar mass by examining the relationship between  $\mathcal{R}$  and  $\log \Sigma$ , as well as comparing the distributions of  $\mathcal{R}$  across low and high-density environments and between low and high-mass galaxies.

### 3 RESULTS

As our sample size is small, with galaxies in the highest-density environments underrepresented, we set cut-offs for the low, intermediate and high-density environments at the 33.3rd and 66.7th percentiles of  $\log \Sigma$  (-0.46 and 0.13, respectively). This approach produces roughly equal-sized density bins. Our low-density bin has a higher cut-off than the  $\log \Sigma < -0.8$  cut-off sometimes used to distinguish voids (Baldry et al. 2006; Mouhcine, Baldry & Bamford 2007). However, it aligns with how isolated galaxies are defined by Iovino et al. (2010), who use the  $-0.8 < \log \Sigma < -0.4$  range. Bamford et al. (2009) apply an even more generous cut-off of  $\log \Sigma < 0$  for low-density environments. Our high-density bin ( $\log \Sigma > 0.13$ ) falls below typical cluster ranges. Mouhcine et al. (2007) use  $\log \Sigma > 0.8$  for inner parts of galaxy clusters and Baldry et al. (2006) use  $\log \Sigma > 0.8$  for cluster-like environments. It also falls below the lower limit for group environments ( $0.4 < \log \Sigma < 0.8$ ) set by Iovino et al. (2010). Therefore, our low, intermediate and high-density labels refer to relative sample density,

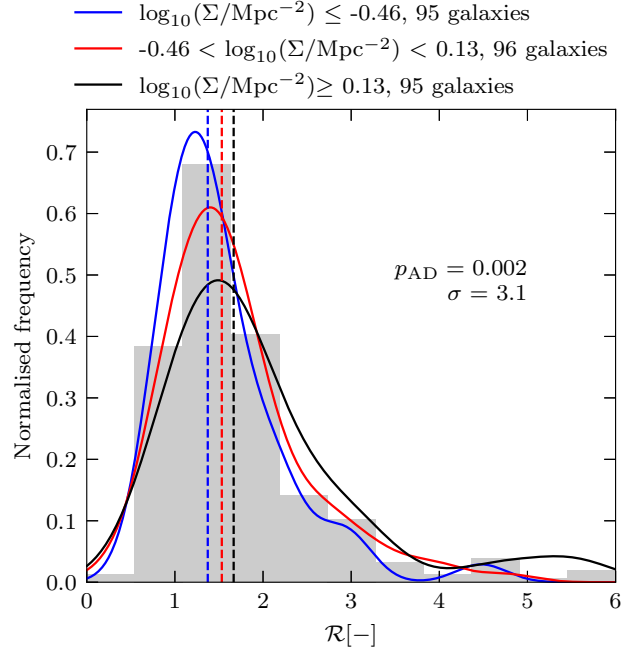


**Figure 1.** Distributions of the bar rotation rate,  $\mathcal{R}$ , for 286 galaxies. The distributions for the low, intermediate and high-density samples fitted with Gaussian kernel estimates are blue, red and black, respectively. The dashed vertical lines indicate the median values of  $\mathcal{R}$  in the samples. The Anderson–Darling  $p$ -value with the null hypothesis being that the  $\mathcal{R}$  values in the low and high-density samples were drawn from the same population is  $p_{\text{AD}} = 0.002$ , a statistically significant result ( $3.1 \sigma$ ). This means that galaxies in low-density environments preferentially host faster bars (with lower  $\mathcal{R}$ ) than galaxies in high-density environments, despite a significant overlap between the two distributions.

with the low-density bin predominantly containing isolated galaxies in void-like regions, and the high-density bin containing a range of dense environments (including groups and clusters).

The distributions of  $\mathcal{R}$  in these environments are shown in Fig. 1. The median values of  $\mathcal{R}$  in the low, intermediate and high-density environments are  $\mathcal{R} = 1.37^{+0.49}_{-0.34}$ ,  $\mathcal{R} = 1.53^{+0.55}_{-0.38}$  and  $\mathcal{R} = 1.67^{+0.72}_{-0.41}$ , respectively. To assess the significance of the difference between the low-density and high-density environments, we perform the Anderson–Darling test. The null hypothesis is that the  $\mathcal{R}$  values in the low and high-density subgroups were drawn from the same population. We obtain a  $p$ -value of  $p_{\text{AD}} = 0.002$ , which corresponds to a  $3.1 \sigma$  result. Since we require at least  $3 \sigma$  for statistical significance, the Anderson–Darling test indicates that bars hosted in galaxies in low-density environments have significantly lower values of  $\mathcal{R}$  (i.e. tend to be faster) than galaxies in high-density environments, despite a big overlap between the two distributions (see Fig. 1).

Fig. 2 shows a scatter plot between  $\mathcal{R}$  and  $\log \Sigma$  along with histograms depicting the distributions of both variables. We see a weak positive trend between  $\mathcal{R}$  and  $\log \Sigma$ . A robust linear regression accounting for intrinsic scatter, obtained with the BCES  $y|x$  method (bivariate correlated errors and intrinsic scatter; Akritas & Bershady 1996), is depicted with the black dashed line. The best-fitting slope between  $\mathcal{R}$  and  $\log \Sigma$  is  $\beta = 0.39 \pm 0.13$  ( $1 \sigma$  uncertainty). To better capture the trend in the data, we calculate the Pearson correlation coefficient between  $\mathcal{R}$  and  $\log \Sigma$  which yields a value of  $r = 0.20$  with  $3.3 \sigma$  significance, confirming a statistically significant weakly positive correlation.

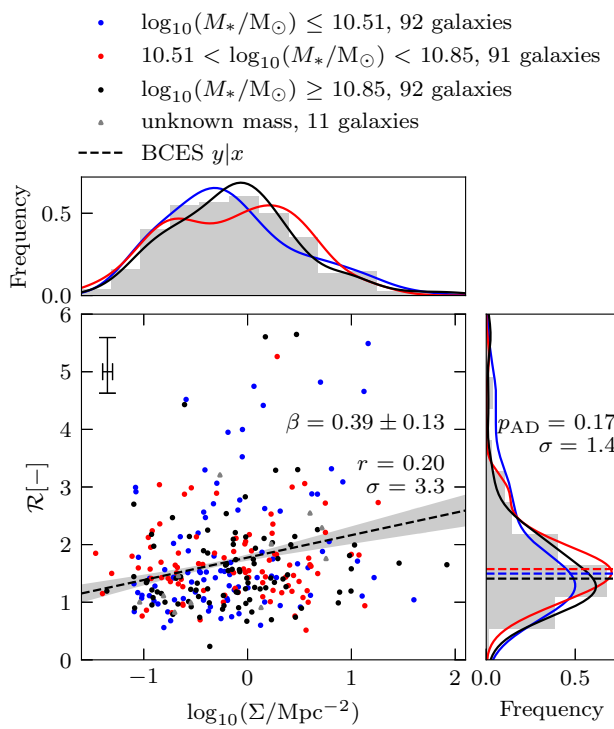


**Figure 2.** Scatter plot of the bar rotation rate,  $\mathcal{R}$ , against projected neighbour density,  $\log \Sigma$ , for 286 galaxies. The error bar represents median errors in  $\mathcal{R}$  and  $\log \Sigma$ . Low, intermediate and high-mass galaxies are coloured blue, red and black, respectively (the same colouring has been used for the histograms). 11 galaxies with unknown mass are coloured grey. The black dashed line shows a robust linear regression obtained with the BCES  $y|x$  method with the grey shaded region representing  $1\sigma$  confidence. The best-fitting slope to the data obtained with this method is  $\beta = 0.39 \pm 0.13$ . The Pearson correlation coefficient between  $\mathcal{R}$  and  $\log \Sigma$  is  $r = 0.20$  with  $3.3\sigma$  significance, indicating a statistically significant weakly positive correlation. The histograms show low, intermediate and high-mass galaxy samples fitted with Gaussian kernel estimates. The Anderson–Darling  $p$ -value with the null hypothesis being that the  $\mathcal{R}$  values in the low and high-mass samples were drawn from the same population is  $p_{AD} = 0.17$  ( $1.4\sigma$ ), so the distributions are not statistically significantly different.

We next examine whether bar rotation rate depends on galaxy stellar mass. In literature, there are no agreed-upon thresholds for galaxy stellar mass which we could use to separate our sample into low, intermediate and high-mass bins. For example, [Sherman et al. \(2020\)](#) use a  $10^{11} M_\odot$  threshold to define high-mass galaxies, while [Pérez et al. \(2025\)](#) use  $10^{10.5} M_\odot$  as a cut-off for low-mass and high-mass galaxies. [Géron et al. \(2021\)](#) refer to the  $M_\star < 10^{10} M_\odot$  range as low. A reasonable threshold is  $M_\star \sim 10^{10.2} M_\odot - 10^{10.3} M_\odot$ , which marks a reversal of bar fraction trends in the local Universe ([Nair & Abraham 2010; Skibba et al. 2012; Mukundan et al. 2025](#)). However, because of the small sample size in our study, we choose to set the cut-offs at the 33.3rd and 66.7th percentiles of  $\log M_\star$ , producing roughly equal-sized galaxy stellar mass bins. This corresponds to galaxy stellar masses of  $10^{10.51} M_\odot$  and  $10^{10.85} M_\odot$ , respectively. Therefore, our low-mass bin is consistent with the one used in [Pérez et al. \(2025\)](#), whereas the high-mass cut-off lies between the ones used by [Sherman et al. \(2020\)](#) and [Pérez et al. \(2025\)](#).

The data in the scatter plot and the histograms in Fig. 2 are coloured based on the 33.3rd and 66.7th percentiles of  $\log M_\star$ . The median values of  $\mathcal{R}$  in the low, intermediate and high-mass subgroups are

$\mathcal{R} = 1.50_{-0.43}^{+0.71}$ ,  $\mathcal{R} = 1.58_{-0.38}^{+0.64}$  and  $\mathcal{R} = 1.41_{-0.33}^{+0.48}$ , respectively. To assess the significance of the difference between the low-mass and high-mass environments, we perform the Anderson–Darling test. The null hypothesis is that the  $\mathcal{R}$  values in the low and high-mass subgroups were drawn from the same population. We obtain a  $p$ -value of  $p_{AD} = 0.17$ , which corresponds to  $1.4\sigma$ , indicating that the distributions do not differ significantly.

The above results suggest that the dynamics of bars depend more strongly on environmental density than on galaxy stellar mass, consistent with theoretical expectations and predictions from simulations.

## 4 DISCUSSION

Studies by [Miwa & Noguchi \(1998\)](#), [Berentzen et al. \(2004\)](#), [Lokas et al. \(2014, 2016\)](#), [Martinez-Valpuesta et al. \(2017\)](#), [Gajda et al. \(2017\)](#) and [Lokas \(2018\)](#) suggest that tidal bars tend to rotate slower with respect to the stellar discs than bars formed by internal disc instabilities, possibly due to angular momentum transfer to the perturber during the interaction, as proposed by [Miwa & Noguchi \(1998\)](#). Since tidal bar formation has been shown to be possible in cluster cores but not in cluster outskirts ([Lokas et al. 2016](#)), we hypothesised that a higher environmental density would lead to a higher fraction of tidally triggered bars. Hence, if tidally triggered bars are slower, measurements of  $\mathcal{R}$  and  $\log \Sigma$  should reveal a positive correlation between the two variables.

To test this prediction with observational data, our approach was to compare the bar rotation rates of 286 galaxies across different environmental densities (see Fig. 1). We have found that bars in high-density environments are significantly slower than bars in low-density environments ( $p_{AD} = 0.002$ ,  $3.1\sigma$ ). Specifically, in dense environments, we have measured the median  $\mathcal{R} = 1.67_{-0.41}^{+0.72}$ , whereas in low-density environments, we have measured it to be  $\mathcal{R} = 1.37_{-0.34}^{+0.49}$ . However, please note the overlap between the distributions in Fig. 1 and the large uncertainties in  $\mathcal{R}$ . A robust linear regression obtained with the BCES  $y|x$  method yielded a best-fitting slope of  $\beta = 0.39 \pm 0.13$  between  $\mathcal{R}$  and  $\log \Sigma$  (see Fig. 2). Additionally, we have calculated the Pearson correlation coefficient between  $\mathcal{R}$  and  $\log \Sigma$  to be  $r = 0.20$  with a  $3.3\sigma$  significance, indicating a statistically significant, albeit weak, positive correlation between  $\mathcal{R}$  and  $\log \Sigma$ . The Pearson correlation, alongside the outcome of the Anderson–Darling test and the BCES  $y|x$  linear regression, suggest that the rotation rates of bars are influenced by the mechanism behind their formation, with denser environments favouring the formation of slower, tidally triggered bars. This is in support of the predictions from simulations by [Miwa & Noguchi \(1998\)](#), [Berentzen et al. \(2004\)](#), [Lokas et al. \(2014, 2016\)](#), [Martinez-Valpuesta et al. \(2017\)](#), [Gajda et al. \(2017\)](#) and [Lokas \(2018\)](#). We note, however, that the Tremaine–Weinberg method can only be applied to galaxies which meet strict criteria. Most importantly, the TW method assumes continuity of the tracer ([Tremaine & Weinberg 1984](#)). This condition will not be met in a galaxy with a disturbed velocity field due to environmental mechanisms (tidal interactions, ram-pressure stripping, etc.). As a result, galaxies in high-density environments often do not meet the criteria for TW and are discarded in bar studies. This may introduce bias against highly disturbed cluster galaxies and may reduce the sensitivity to the effects of extremely dense environments on bar rotation rates.

To test whether galaxy stellar mass could be responsible for variations in  $\mathcal{R}$ , we compared the distributions of  $\mathcal{R}$  across low, intermediate and high-mass barred galaxies, with their median values of  $\mathcal{R}$  being  $\mathcal{R} = 1.50_{-0.43}^{+0.71}$ ,  $\mathcal{R} = 1.58_{-0.38}^{+0.64}$  and  $\mathcal{R} = 1.41_{-0.33}^{+0.48}$ , respec-

tively. The Anderson–Darling test revealed no significant differences between the distributions of  $\mathcal{R}$  in the low and high-mass subgroups ( $p_{AD} = 0.17, 1.4\sigma$ ; see Fig. 2). It is however important to note the small sample size in this study. This issue could be addressed by increasing the sample size of barred galaxies for which galaxy stellar mass is known and focusing specifically on the relationship between galaxy stellar mass and bar rotation rate. The upcoming Integral Field Unit survey conducted by Hector (Bryant et al. 2020) is of particular interest, as it aims to survey approximately 15,000 galaxies. Assuming that due to the constraints on the TW method only 2 per cent of the data are retained, this would allow to add roughly 300 galaxies to the sample.

## 5 CONCLUSIONS

We have used the estimates of  $\mathcal{R}$  obtained with the Tremaine–Weinberg method applied to IFU spectroscopy from SDSS MaNGA and CALIFA across six studies (Aguerri et al. 2015; Guo et al. 2019; Cuomo et al. 2019; Garma-Oehmichen et al. 2020, 2022; Géron et al. 2023). Our sample consisted of 334 galaxies in the local Universe ( $0.017 < z < 0.078$ ), which we cross-matched with catalogues containing environmental densities (Baldry et al. 2006) and galactic stellar masses (Kauffmann et al. 2003), marking the first empirical test of the assumption that fast bars are formed by global instabilities in the galaxy disc, while slow bars are triggered by tidal interactions. We have found significant evidence that the rotation rates of bars are influenced by the mechanism behind their formation. Despite a significant overlap in the low-density and high-density distributions, denser environments favour the formation of slower, tidally triggered bars ( $p_{AD} = 0.002, 3.1\sigma$ ). Specifically, we have measured the median  $\mathcal{R}$  in low ( $\log \Sigma \leq -0.46$ ) and high-density ( $\log \Sigma \geq 0.13$ ) environments to be  $\mathcal{R} = 1.37^{+0.49}_{-0.34}$  and  $\mathcal{R} = 1.67^{+0.72}_{-0.41}$ , respectively. Additionally, we have found no evidence suggesting significant differences in the bar pattern speed between low and high-mass galaxies.

These results will be solidified by new Integral Field Unit data. An exciting upcoming survey will be conducted by Hector, a spectrograph installed on the Anglo-Australian Telescope. Hector aims to survey approximately 15,000 galaxies up to 2 effective radii (Bryant et al. 2020). This extensive survey will significantly increase the number of galaxies to which the Tremaine–Weinberg method can be applied, adding roughly 300 galaxies to the sample in this paper. We encourage observations of barred galaxies with IFUs as a means of providing insight into their formation and evolution.

## DATA AVAILABILITY

This research has made use of publicly available data. The  $\mathcal{R}$  data were obtained from six independent sources: Géron et al. (2023) (<https://zenodo.org/records/7567945>), Garma-Oehmichen et al. (2022) ([https://github.com/lgarma/MWA\\_pattern\\_speed](https://github.com/lgarma/MWA_pattern_speed)), Garma-Oehmichen et al. (2020, Table 4), Guo et al. (2019, Table 4) (values taken from column  $\mathcal{R}_1$ ), Cuomo et al. (2019, Table 2) and Aguerri et al. (2015, Table 4) (values taken from column  $\mathcal{R}_1$ ). Measurements of stellar masses ( $\log M_\star$ ) and neighbour density ( $\log \Sigma$ ) were taken from publicly available catalogues cited in the text.

## REFERENCES

Abazajian K. N., et al., 2009, *ApJS*, **182**, 543  
 Abdurro'uf et al., 2022, *ApJS*, **259**, 35  
 Aguerri J. A. L., et al., 2015, *A&A*, **576**, A102  
 Aguerri J. A. L., Cuomo V., Rojas-Roncero A., Morelli L., 2023, *A&A*, **679**, A5  
 Akritas M. G., Bershady M. A., 1996, *ApJ*, **470**, 706  
 Amvrosiadis A., et al., 2025, *MNRAS*, **537**, 1163  
 Athanassoula E., 2013, in Falcón-Barroso J., Knapen J. H., eds, , Secular Evolution of Galaxies. Proceedings of the XXIII Canary Islands Winter School of Astrophysics. Cambridge Univ. Press, Cambridge, p. 305  
 Athanassoula E., Machado R. E. G., Rodionov S. A., 2013, *MNRAS*, **429**, 1949  
 Baldry I. K., Balogh M. L., Bower R. G., Glazebrook K., Nichol R. C., Bamford S. P., Budavari T., 2006, *MNRAS*, **373**, 469  
 Bamford S. P., et al., 2009, *MNRAS*, **393**, 1324  
 Berentzen I., Athanassoula E., Heller C. H., Fricke K. J., 2004, *MNRAS*, **347**, 220  
 Bland-Hawthorn J., Tepper-Garcia T., Agertz O., Freeman K., 2023, *ApJ*, **947**, 80  
 Bryant J. J., et al., 2020, in Evans C. J., Bryant J. J., Motohara K., eds, Proc. SPIE Conf. Ser. Vol. 11447, Ground-based and Airborne Instrumentation for Astronomy VIII. SPIE, Bellingham, p. 1144715  
 Bundy K., et al., 2015, *ApJ*, **798**, 7  
 Cavanagh M. K., Bekki K., 2020, *A&A*, **641**, A77  
 Cheung E., et al., 2013, *ApJ*, **779**, 162  
 Combes F., 2009, in Jogee S., Marinova I., Hao L., Blanc G. A., eds, ASP Conference Series Vol. 419, Active Galaxies. Galaxy Evolution: Emerging Insights and Future Challenges. Astron. Soc. Pac., San Francisco, p. 31  
 Combes F., Sanders R. H., 1981, *A&A*, **96**, 164  
 Contopoulos G., 1980, *A&A*, **81**, 198  
 Costantin L., et al., 2023, *Nature*, **623**, 499  
 Cuomo V., Lopez Aguerri J. A., Corsini E. M., Debattista V. P., Méndez-Abreu J., Pizzella A., 2019, *A&A*, **632**, A51  
 Erwin P., 2018, *MNRAS*, **474**, 5372  
 Eskridge P. B., et al., 2000, *AJ*, **119**, 536  
 Font J., et al., 2017, *ApJ*, **835**, 279  
 Fried J. W., 1988, *A&A*, **189**, 42  
 Fujii M. S., Bédorf J., Baba J., Portegies Zwart S., 2018, *MNRAS*, **477**, 1451  
 Gajda G., Łokas E. L., Athanassoula E., 2017, *ApJ*, **842**, 56  
 Garma-Oehmichen L., Cano-Díaz M., Hernández-Toledo H., Aquino-Ortíz E., Valenzuela O., Aguerri J. A. L., Sánchez S. F., Merrifield M., 2020, *MNRAS*, **491**, 3655  
 Garma-Oehmichen L., et al., 2022, *MNRAS*, **517**, 5660  
 Géron T., 2023, PhD thesis, University of Oxford  
 Géron T., Smethurst R. J., Lintott C., Kruk S., Masters K. L., Simmons B., Stark D. V., 2021, *MNRAS*, **507**, 4389  
 Géron T., et al., 2023, *MNRAS*, **521**, 1775  
 Géron T., et al., 2025, *ApJ*, **987**, 74  
 Ghosh S., Saha K., Di Matteo P., Combes F., 2021, *MNRAS*, **502**, 3085  
 Guo R., Mao S., Athanassoula E., Li H., Ge J., Long R. J., Merrifield M., Masters K., 2019, *MNRAS*, **482**, 1733  
 Hohl F., 1971, *ApJ*, **168**, 343  
 Iovino A., et al., 2010, *A&A*, **509**, A40  
 Kauffmann G., et al., 2003, *MNRAS*, **341**, 33  
 Kraljic K., Bournaud F., Martig M., 2012, *ApJ*, **757**, 60  
 Kruk S. J., et al., 2018, *MNRAS*, **473**, 4731  
 Kumar A., Das M., Kataria S. K., 2022, *MNRAS*, **509**, 1262  
 Kyzliopoulos P. E., Efthymiopoulos C., Gravvanis G. A., Patsis P. A., 2016, *MNRAS*, **463**, 2210  
 Lang M., Holley-Bockelmann K., Sinha M., 2014, *ApJ*, **790**, L33  
 Łokas E. L., 2018, *ApJ*, **857**, 6  
 Łokas E. L., Athanassoula E., Debattista V. P., Valluri M., Pino A. d., Semczuk M., Gajda G., Kowalczyk K., 2014, *MNRAS*, **445**, 1339  
 Łokas E. L., Ebrová I., del Pino A., Sybilska A., Athanassoula E., Semczuk M., Gajda G., Fouquet S., 2016, *ApJ*, **826**, 227

Martinez-Valpuesta I., Shlosman I., 2004, [ApJ, 613, L29](#)

Martinez-Valpuesta I., Shlosman I., Heller C., 2006, [ApJ, 637, 214](#)

Martinez-Valpuesta I., Aguerri J. A. L., González-García A. C., Dalla Vecchia C., Stringer M., 2017, [MNRAS, 464, 1502](#)

Masters K. L., et al., 2011, [MNRAS, 411, 2026](#)

Masters K. L., et al., 2012, [MNRAS, 424, 2180](#)

Melvin T., et al., 2014, [MNRAS, 438, 2882](#)

Miwa T., Noguchi M., 1998, [ApJ, 499, 149](#)

Moetazedian R., Polyachenko E. V., Berczik P., Just A., 2017, [A&A, 604, A75](#)

Mouhcine M., Baldry I. K., Bamford S. P., 2007, [MNRAS, 382, 801](#)

Mukundan K., Nair P., Masters K. L., Bailin J., Gwartney P., Li W., 2025, [MNRAS, 542, 151](#)

Nair P. B., Abraham R. G., 2010, [ApJ, 714, L260](#)

Noguchi M., 1987, [MNRAS, 228, 635](#)

Ostriker J. P., Peebles P. J. E., 1973, [ApJ, 186, 467](#)

Pérez I., et al., 2025, [A&A, 695, A84](#)

Raha N., Sellwood J. A., James R. A., Kahn F. D., 1991, [Nature, 352, 411](#)

Rautiainen P., Salo H., Laurikainen E., 2008, [MNRAS, 388, 1803](#)

Rosas-Guevara Y., et al., 2020, [MNRAS, 491, 2547](#)

Sánchez S. F., et al., 2012, [A&A, 538, A8](#)

Sarkar S., Pandey B., Bhattacharjee S., 2021, [MNRAS, 501, 994](#)

Sellwood J. A., 2012, [ApJ, 751, 44](#)

Sellwood J. A., 2014, [Rev. Mod. Phys., 86, 1](#)

Sherman S., et al., 2020, [MNRAS, 491, 3318](#)

Sheth K., et al., 2008, [ApJ, 675, 1141](#)

Skibba R. A., et al., 2012, [MNRAS, 423, 1485](#)

Smail I., et al., 2023, [ApJ, 958, 36](#)

Tremaine S., Weinberg M. D., 1984, [ApJ, 282, L5](#)

Walmsley M., et al., 2023, [MNRAS, 526, 4768](#)

This paper has been typeset from a  $\text{\TeX}/\text{\LaTeX}$  file prepared by the author.